

Toward a Fracture Mechanics–Based Design Approach for Unbonded Concrete Overlay Pavements

Minmao Liao, Ph.D., S.M.ASCE¹; and Roberto Ballarini, Ph.D., P.E., F.ASCE²

Abstract: An illustrative fracture mechanics–based design paradigm is proposed for unbonded concrete overlays (UBCOs), an increasingly popular pavement rehabilitation system, with the ultimate goal of establishing a more rational design procedure than those currently available. To illustrate the advantages of the fracture mechanics–based approach to design, specific attention is paid to one type of failure associated with pavement structures, reflection cracking. The design formulas derived from the results of a large number of crack propagation simulations of both the UBCO composite and a reference single-layer new pavement quantify the dependence of the required overlay thickness and load-carrying capacity on all relevant material and geometric parameters. Preliminary comparisons of the results with field observations suggest that the fracture mechanics paradigm offers a promising procedure for improved design of UBCOs. DOI: [10.1061/\(ASCE\)EM.1943-7889.0000412](https://doi.org/10.1061/(ASCE)EM.1943-7889.0000412). © 2012 American Society of Civil Engineers.

CE Database subject headings: Concrete pavements; Pavement overlays; Design; Composite structures; Cracking; Finite element method; Equivalence.

Author keywords: Pavement overlays; Composite structures; Cracking; Finite-element method; Equivalence.

Introduction

Large increases in traffic and the end of the service life of a significant number of existing pavements in the United States have produced a growing demand for highway pavement rehabilitation. Among various rehabilitation techniques, unbonded concrete overlays (UBCOs) are likely to become increasingly popular because numerous states have found that they perform well when properly designed. UBCOs are cost effective and durable, mitigate reflection cracking, require minimal preoverlay preparation, can be placed quickly and efficiently, and are recyclable. UBCOs have been used since the 1910s to restore ride quality, provide an appropriate surface texture, restore or increase load-carrying capacity, and extend the life of existing pavements. The current design procedures for UBCOs are based on empirical equations or highly simplified mechanistic models. In fact, the design procedures used for UBCOs for highway pavements have mirrored those developed for airfield pavements that are subjected to qualitatively and quantitatively different loading. The concern is that the current designs may require overly conservative overlay thicknesses and, thus, reduce cost effectiveness.

An UBCO system, as shown in Fig. 1(a), consists of the existing damaged portland cement concrete (PCC) pavement, a thin asphalt concrete (AC) interlayer, and a new PCC overlay. It is assumed (however, it has not been demonstrated) that the 2.54–5.08-cm-thick

interlayer allows relative deformation between the overlay and the existing pavement, and serves to prevent the reflection cracking of the overlay that is associated with bonded concrete overlays (BCOs). Consequently, UBCOs can be used for badly damaged existing pavements, thereby minimizing preoverlay repairs and reducing construction costs. An additional advantage of UBCOs in applications involving severely damaged foundations is that (unlike BCOs) their joints are not required to line up with those of the existing pavement. In fact, specific joint mismatching is usually recommended to provide a sleeper slab arrangement, which improves load transfer. Finally, UBCOs can be used under any traffic level and climate scenario.

Construction of UBCOs is similar to that of conventional PCC pavements and does not require specialized equipment. However, special attention should be given to geometric constraints such as overhead vertical clearances. According to Minnesota's experience (Engstrom 1993), compared with US \$500,000 for reconstructed PCC pavements, UBCOs cost only around US \$350,000 per two lanes per mile. Therefore, with the advances in paving materials and paving technology, UBCOs are becoming more attractive as an alternative for highway pavement rehabilitation.

For a given set of material properties, the required overlay thickness is determined using several empirical and simplified mechanistic design procedures. For example, the Minnesota Department of Transportation (MnDOT 1993) relies on the empirical methods developed by the Departments of the Army and the Air Force (DA/DAF 1970) and the mechanistic models proposed by Tayabji and Okamoto (1985). Detailed descriptions of the two procedures are provided in the appendix. Because pavement engineers have developed relatively robust design procedures for new single-layer pavements consisting of a PCC slab on a foundation, the structural equivalency design paradigm has been proposed to design UBCOs. A similar approach is adopted here. This procedure demands that the thickness of the UBCO be such that it attains the same value of a certain metric as does a single-layer pavement designed for the same service conditions. Some of the currently available mechanistic designs, including the Tayabji and Okamoto

¹Graduate Student, Dept. of Civil Engineering, Univ. of Minnesota, Minneapolis, MN 55455. E-mail: liaox069@umn.edu

²Professor, Dept. of Civil Engineering, Univ. of Minnesota, Minneapolis, MN 55455 (corresponding author). E-mail: roberto@umn.edu

Note. This manuscript was submitted on October 27, 2011; approved on February 10, 2012; published online on February 13, 2012. Discussion period open until February 1, 2013; separate discussions must be submitted for individual papers. This paper is part of the *Journal of Engineering Mechanics*, Vol. 138, No. 9, September 1, 2012. ©ASCE, ISSN 0733-9399/2012/9-1195–1204/\$25.00.

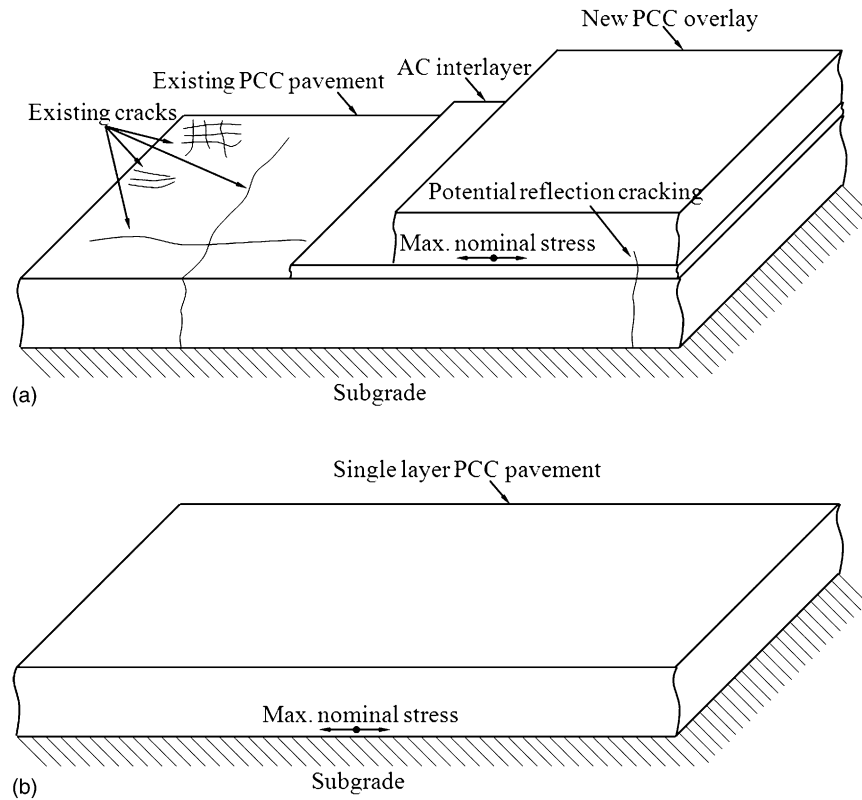


Fig. 1. (a) Schematic of an UBCO system; (b) stress equivalency

(1985) procedure, use stress equivalency [Fig. 1(b)]; the maximum nominal stress in the UBCO and the single-layer pavement should be equal. However, such stress-based material failure theories are not capable of quantifying the loads required to initiate and propagate the reflection cracks that emanate from singular stress-producing cracklike features in the existing PCC pavement. This paper focuses precisely on this type of potential pavement failure through a two-dimensional cohesive zone (fracture mechanics) model (CZM) that relates the ultimate load capacity of the UBCO structure to the fundamental material properties and geometric dimensions, captures the well-known size effect in quasi-brittle materials, and eliminates the mesh size dependence that is present in existing stress-based mechanistic models. The comparison of the results obtained from the design formulas derived from the large number of fracture simulations suggest that the fracture mechanics-based paradigm offers promise for developing more robust design procedures and determining if it is possible to reduce overlay thickness requirements through selection of material properties and structural geometry.

Fracture Mechanics–Based Structural Equivalency Approach

The metric chosen here for structural equivalency is not a nominal stress within the pavement, it is the maximum load achieved during the failure simulation of the two structures shown in Fig. 2. A single-layer pavement resting on a foundation that, under the action of a monotonically increasing point force, experiences the initiation and propagation of a crack at the location of maximum nominal stress in the initially uncracked configuration is illustrated on the right-hand side in Fig. 2. A three-layer UBCO system that, under similar loading, fails as a result of a reflection crack that forms at the

tip of a cracklike feature representing a preexisting crack or joint in the existing pavement is illustrated on the left-hand side in Fig. 2. The load-carrying capacities of both structures are determined from the results of the CZM. The UBCO and the single layer are deemed structurally equivalent if they have equal load-carrying capacity. Consequently, the proposed thickness design procedure for an UBCO is as follows. For the prescribed service requirements, a new single-layer PCC pavement is designed according to the currently available robust procedures. The ultimate load capacity of the design is determined from a CZM failure simulation. The thickness and/or material properties of the UBCO are, in turn, determined to render it structurally equivalent to the single-layer configuration.

The remaining part of this paper is divided into four sections. The first two present the results of the CZM simulations of the single-layer and UBCO pavements, respectively. The third section derives and discusses the implications of the design formulas produced from the structural equivalency concept. The final section compares the implications with observations of UBCOs tested at the MnROAD test facility in Minnesota.

Single-Layer PCC Pavement

The plane strain model of a single-layer PCC pavement of length, L , depth, h , and thickness, b , resting on a Winkler foundation (Westergaard 1947) with stiffness, k , is shown in Fig. 3. For the illustrative purposes of this paper, the pavement is assumed to carry a concentrated vertical force at midspan and to be fully bonded with the foundation. Thus, potential separation between the pavement and the foundation is not simulated. In addition, pavement joint load transfer is not considered in this paper; the ends of the pavement are free to rotate. Failure is assumed to result from the initiation

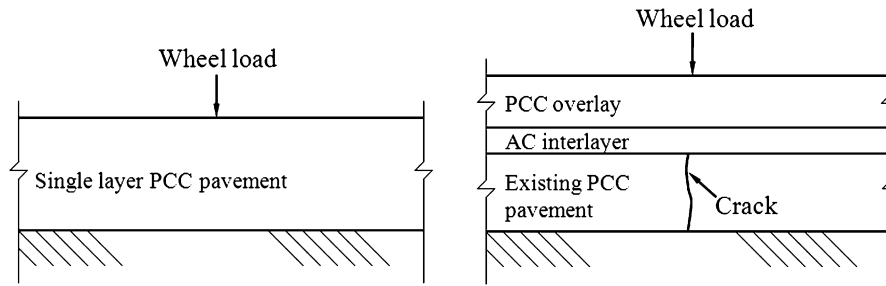


Fig. 2. Proposed structurally equivalent structures

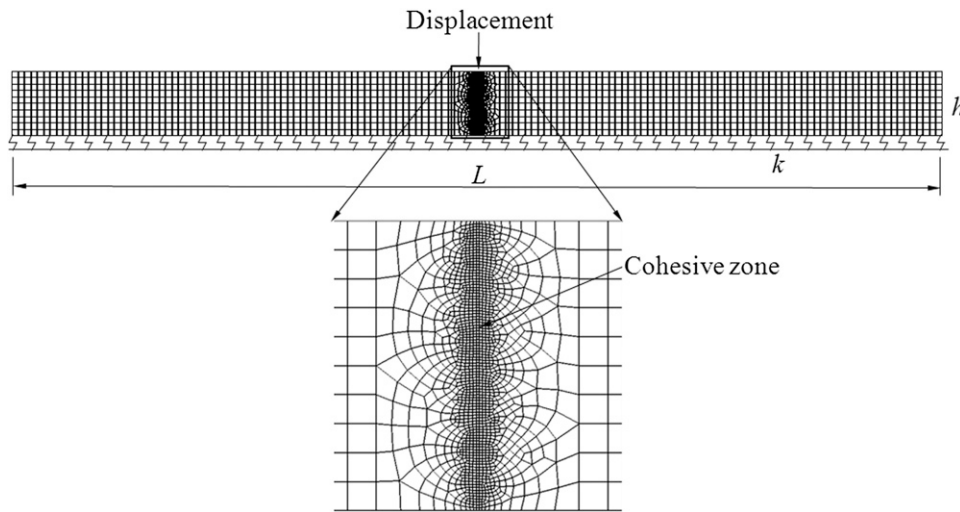


Fig. 3. CZM of a single-layer PCC pavement

and subsequent propagation of a cohesive edge crack at the point of maximum tensile stress. The CZM assumes that the crack opening displacement at each point along the crack surfaces, δ , is resisted by a conjugate traction, σ . As shown by Petersson (1981), Wittmann et al. (1988), Hilsdorf and Bramshuber (1991), and Roesler et al. (2007), concrete is best described using a bilinear softening traction-separation relationship. A bilinear relationship similar to the one proposed by Wittmann et al. (1988) (shown in Fig. 4) is adopted in this paper. The fracture energy, G_F , is defined by the tensile strength, f_t , and the critical crack opening displacement, δ_c . The coordinates of the kink point are $0.125\delta_c$, and $0.25f_t$. According to Bažant (2002), the initial fracture energy (the area under the first descending slope of the softening curve) controls the maximum load of ordinary concrete structures. The remaining portion of the fracture energy determines the postpeak behavior. As discussed in detail in Bažant and Planas (1998) and Bažant and Novak (2001), the f_t in the cohesive law is a fundamental property of the material, and should not be confused with the modulus of rupture (MOR) that the pavement community determines using the ASTM standard for flexural strength. Bažant and Planas (1998) provide a review of numerous experiments that drive home the point that the MOR is strongly dependent on specimen size. Therefore, all the results presented in this paper should be understood in terms of an f_t that at some point needs to be measured independently or be experimentally correlated with a size-dependent flexural strength. It is also important to note that in the illustrative examples presented in this paper a constant $\delta_c = 0.2 \text{ mm}$ is used. This is justified by the fact that only the ultimate capacity is of interest. Moreover, it is noted that the change in abscissa of the

kink point, which quantifies the first portion of the fracture energy that controls capacity, is equal to only one-eighth of the change in abscissa of δ_c . Maintaining a constant δ_c renders the total fracture energy G_F a function only of f_t .

The cohesive zone is implemented using the concrete damaged plasticity material properties in ABAQUS [Dassault Systèmes Simulia Corporation (SIMULIA) 2010], for which the $\sigma - \delta$ relationship is input in tabular form. The material model involves a scalar tension damage parameter indicating the extent of fracture varying from 0 to 1 that is also input as a tabular function of δ . The damage parameter is set equal to zero when the crack opening displacement is zero and 0.9 when δ reaches δ_c . The aspect ratio of the elements within the cohesive zone is made equal to 1.0 to mitigate mesh sensitivity. Details of the modeling approach, including the choice of the value of the damage parameters and mesh density that guaranteed convergence of the peak loads to within a few percent, can be recovered in Liao (2011). It is noted that the symmetry conditions were not applied because the large number of geometry discretizations that were constructed as part of the parameter study will be used in the near future for nonsymmetric loadings.

The fracture energy introduces a characteristic length, which is proportional to the length of the process zone in the vicinity of the crack front, defined by

$$l_{ch} = \frac{EG_F}{f_t^2} \quad (1)$$

where E = Young's modulus. In general, a quasi-brittle structure is expected to behave in a brittle manner if h/l_{ch} is large and in

a ductile manner if it is small. However, in subsequent simulations the magnitude of the fracture energy is increased through an increase in tensile strength, which concomitantly increases the magnitude of the slope in the first portion of the traction-separation law shown in Fig. 4.

A 2.54-mm-thick cohesive zone was placed at the midspan of the slab through the whole depth to simulate crack initiation and propagation under displacement control. First-order quadrilateral plane strain elements, designated as CPE4 in ABAQUS, were assigned to all elements. The elements outside the cohesive zone were linear elastic. The algorithm used to solve the finite-element equations relied on the Riks method because it is capable of capturing the snap-back instabilities associated with relatively high values of h/l_{ch} .

Fig. 5 illustrates the CZM's ability to capture the localized deformation in the region that initiates the crack for the illustrative

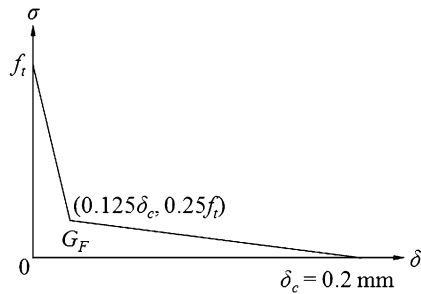


Fig. 4. Bilinear traction-separation relationship of concrete

parameters, $L = 3.66$ m, $h = 0.25$ m, $E = 27.58$ GPa, $f_t = 3.10$ MPa, $G_F = 118.21$ N/m, $k = 27.14$ MPa/m, and Poisson's ratio $\nu = 0.20$. These plots show the $2,000\times$ -amplified mesh deformation, upon which the horizontal stress component contours (in units of psi), σ_{xx} , are superimposed. Four instants of the loading history are shown. Fig. 5(a) corresponds to the unloaded reference state. Fig. 5(b) shows the point at which the tensile stress at the trail end of the cohesive zone reaches the tensile strength, f_t . At this point, where the reaction force at the loaded nodes is approximately 74% of the maximum load, P_{ult} , the cohesive zone starts to unzip. In Fig. 5(c) at $0.9P_{ult}$ the cohesive elements are clearly stretched and in Fig. 5(d) the load capacity P_{ult} is reached.

The structural system of the single-layer pavement involves the physical parameters P_{ult} , L , b , h , E , f_t , G_F , and k . Because G_F is a function of only f_t , the other seven physical parameters are independent. They are expressible in terms of three independent fundamental physical quantities: mass, length, and time. Buckingham's π theorem (Buckingham 1914) states that if a system involves n physical parameters that are expressible in terms of m independent fundamental physical quantities, then $n - m$ dimensionless parameters are required to fully describe the system. Therefore, four dimensionless parameters are required for the single-layer pavement. The following normalization choices reduce subsequent parameter studies. All dimensions are normalized with respect to L , l_{ch} , and the radius of relative stiffness

$$l = \sqrt[4]{\frac{D}{k}} \quad (2)$$

where

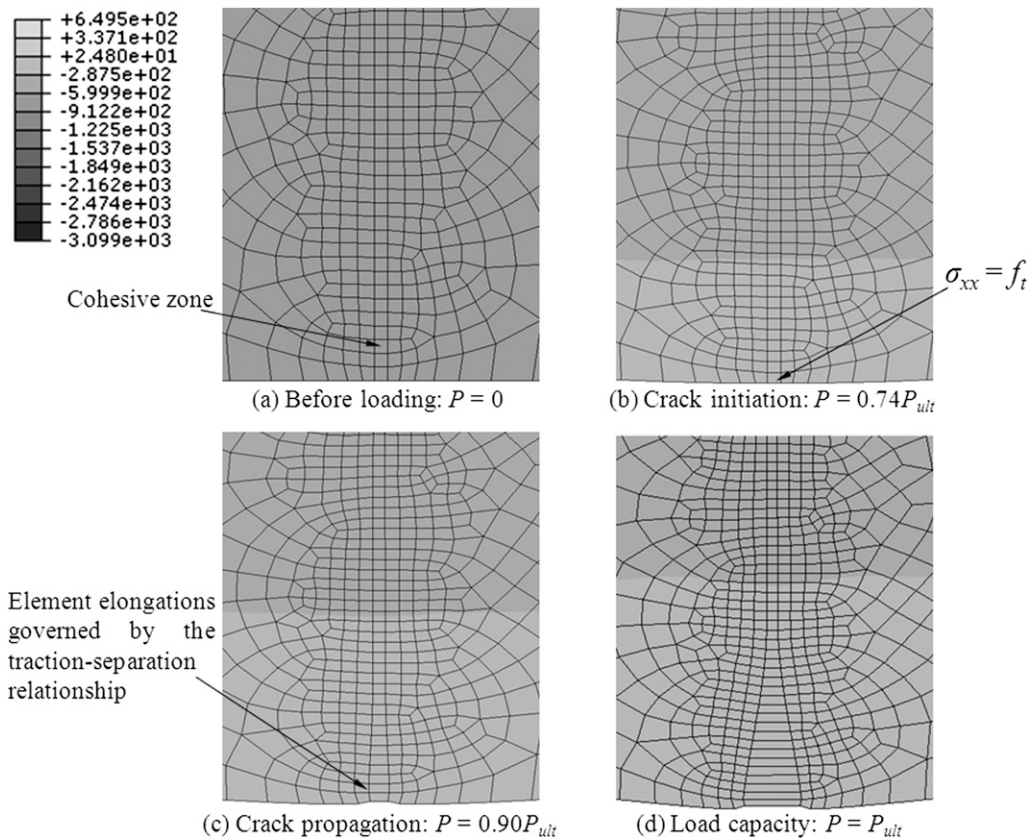


Fig. 5. Deformation and tensile stress distribution along the cohesive zone

$$D = \frac{Eh^3}{12(1-\nu^2)} \quad (3)$$

In the absence of the Winkler foundation, three dimensionless parameters are required: h/L , h/l_{ch} , and the normalized load capacity. The normalized load capacity is defined as the ratio of the MOR to f_t and is written in terms of the maximum bending moment at the midspan, M_{ult} , as

$$\frac{6M_{ult}}{bh^2f_t} = \frac{3P_{ult}L}{2bh^2f_t}$$

Because the influence of h/L is insignificant for relatively slender beams (Ioannides and Sengupta 2003), the normalized load capacity is plotted as a function of h/l_{ch} in Fig. 6. This plot illustrates the well-known transition from ductile to brittle structural response of quasi-brittle materials. The curve can be approximated by the equation

$$\frac{3P_{ult}L}{2bh^2f_t} = 3.76\left(\frac{h}{l_{ch}}\right)^4 - 9.33\left(\frac{h}{l_{ch}}\right)^3 + 8.74\left(\frac{h}{l_{ch}}\right)^2 - 3.84\left(\frac{h}{l_{ch}}\right) + 2.04 \quad (4)$$

In the presence of the Winkler foundation, the maximum bending moment at the midspan (Boresi and Schmidt 2003) is written as

$$M_{ult} = \frac{\sqrt[4]{4(1-\nu^2)}}{4} P_{ult}l\Phi \quad (5)$$

where

$$\Phi = \frac{\cosh\left[\frac{1}{\sqrt[4]{4(1-\nu^2)}}\frac{L}{l}\right] - \cos\left[\frac{1}{\sqrt[4]{4(1-\nu^2)}}\frac{L}{l}\right]}{\sinh\left[\frac{1}{\sqrt[4]{4(1-\nu^2)}}\frac{L}{l}\right] + \sin\left[\frac{1}{\sqrt[4]{4(1-\nu^2)}}\frac{L}{l}\right]} \quad (6)$$

accounts for the finite length of the slab. Consequently, the natural choice for the normalized load capacity is

$$\frac{6M_{ult}}{bh^2f_t} = \frac{3\sqrt[4]{4(1-\nu^2)}P_{ult}l\Phi}{2bh^2f_t}$$

which is plotted in Fig. 6 for practical values of $h/l = 0.21, 0.27$, and 0.32 , respectively. In addition, Fig. 6 shows the sensitivity of the normalized load capacity on h/l for constant values of h/l . The results suggest that for the practical range of the relevant parameters, the various curves of this choice of normalized capacity can be collapsed into the following equation:

$$\frac{3\sqrt[4]{4(1-\nu^2)}P_{ult}l\Phi}{2bh^2f_t} = 5.41\left(\frac{h}{l_{ch}}\right)^4 - 13.44\left(\frac{h}{l_{ch}}\right)^3 + 12.56\left(\frac{h}{l_{ch}}\right)^2 - 5.40\left(\frac{h}{l_{ch}}\right) + 2.35 \quad (7)$$

UBCO Pavement

The configuration and finite-element model of the UBCO is shown in Fig. 7. The PCC overlay, AC interlayer, and existing PCC pavement have thicknesses h_o, h_i , and h_e , and material properties $E_o, E_i, E_e, f_{io}, f_{ii}, G_{Fo}$, and G_{Fi} , respectively. The ends of each layer are free to rotate and, thus, are representative of pavements with zero joint load transfer efficiency. Between each layer, the interfaces are fully bonded to represent the cohesion of the AC interlayer. The separation between the foundation and the existing pavement is not considered. It is important to note that additional types of loadings on the single-layer PCC pavement and on the UBCO system may have significant effects and need to be considered in future analyses. These include geometric imperfections, such as vertical offsets between both sides of the existing pavement in the UBCO system, and the magnitude and distribution across the thickness of the residual stresses produced by shrinkage and changes in temperature.

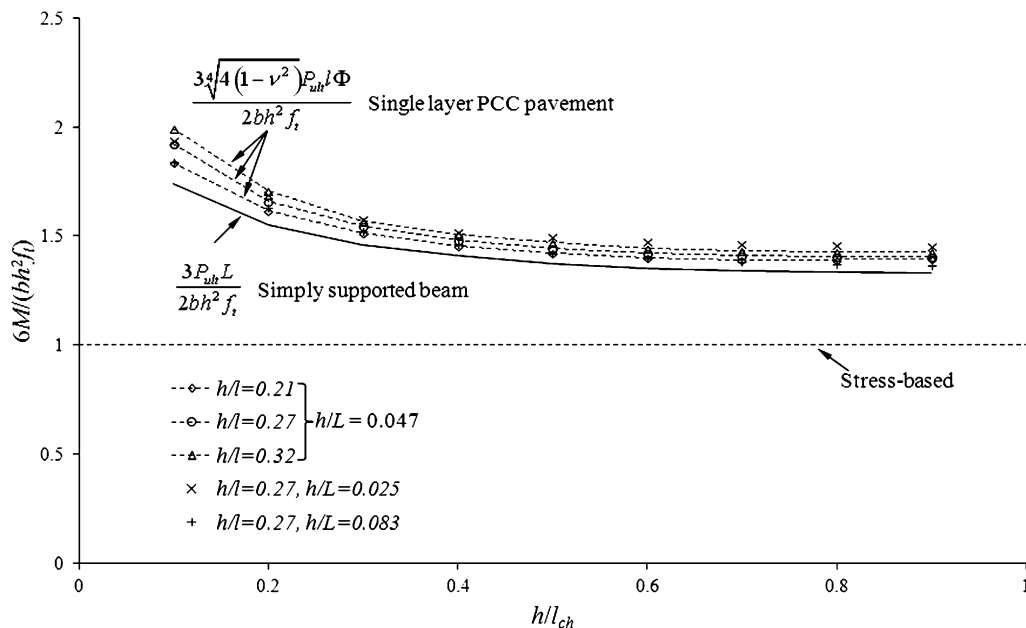


Fig. 6. Normalized load-carrying capacity versus h/l_{ch}

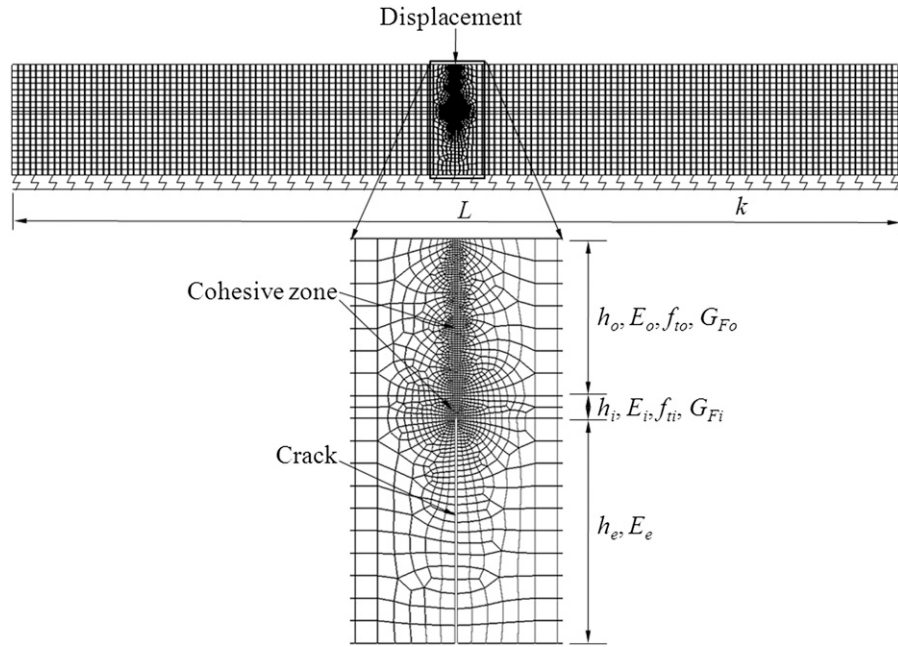


Fig. 7. CZM of an UBCO pavement

The cohesive laws of the overlay and the interlayer have equal shapes as the one used for the single-layer pavement. However, a larger critical crack opening displacement $\delta_c = 0.5$ mm is used for AC. It is noted once again that the simulations and approach presented subsequently are illustrative and quantitatively correct only for the assumed values of critical crack opening displacements of the asphalt and concrete layers.

Reflection cracking within the overlay is assumed to initiate from one preexisting 2.54-mm-thick crack at the midspan of the existing PCC pavement. Note that in the simulations cracking could initiate and propagate through the interlayer before cracking initiated in the overlay, or cracking could initiate in the overlay before cracking in the interlayer propagated through the interlayer, depending on the relative values of fracture toughness.

The UBCO composite involves many more physical parameters than the single-layer PCC pavement; i.e., P_{ult} , b , L , k , h_o , h_i , h_e , E_o , E_i , E_e , f_{io} , f_{ii} , G_{Fo} , and G_{Fi} . Because G_{Fo} and G_{Fi} are functions of f_{io} and f_{ii} , respectively, 12 physical parameters are independent. According to the Buckingham's π theorem, nine dimensionless parameters are necessary to fully describe the system. The normalized load capacity is $P_{ult}/bh_o f_{io}$, and it is a function of the following eight dimensionless quantities: h_o/l_{cho} , h_i/l_{chi} , E_o/E_i , E_o/E_e , h_o/h_i , h_o/h_e , h_o/L , and kh_o/E_o , where l_{cho} and l_{chi} are the characteristic lengths of the PCC overlay and the AC interlayer, respectively.

The results of the large number of fracture simulations demonstrated that for fixed values of overlay thickness, h_o , a combination of power-law and polynomial relationships existed between the remaining dimensionless variables and the load-carrying capacity. The results presented subsequently, for $h_o = 10.16$, 12.70, 15.24, 17.78, and 20.32 cm, respectively, were calculated by consecutively sweeping through a practical range of one independent variable while keeping the rest constant. The ranges of the parameters were the following: $L = 3.66$ – 6.10 m, $k = 27.14$ – 81.43 MPa/m, $h_i = 1.27$ – 5.08 cm, $h_e = 15.24$ – 30.48 cm, $E_o = 27.58$ GPa, $E_i = 3.45$ – 10.34 GPa, $E_e = 34.47$ – 62.05 GPa, $f_{io} = 2.76$ – 4.14 MPa, $f_{ii} = 2.76$ – 4.14 MPa, $G_{Fo} = 105.08$ – 157.61 N/m, and $G_{Fi} = 262.69$ – 394.04 N/m. Using a least-squares analysis gave the following the relationships.

For $h_o = 10.16$ cm:

$$\frac{P_{ult}}{bh_o f_{io}} = 10^4 \left(\frac{h_o}{l_{cho}} \right)^{-0.60} \left(\frac{h_i}{l_{chi}} \right)^{0.49} \left(\frac{E_o}{E_i} \right)^{-0.30} \left(\frac{E_o}{E_e} \right)^{0.05} \left(\frac{h_o}{h_i} \right)^{0.13} \times \left(\frac{h_o}{h_e} \right)^{0.01} \left(\frac{kh_o}{E_o} \right)^{0.54} \left[8.4667 \left(\frac{h_o}{L} \right)^2 - 0.4860 \left(\frac{h_o}{L} \right) + 0.0101 \right] \quad (8a)$$

For $h_o = 12.70$ cm:

$$\frac{P_{ult}}{bh_o f_{io}} = 10^4 \left(\frac{h_o}{l_{cho}} \right)^{-0.62} \left(\frac{h_i}{l_{chi}} \right)^{0.50} \left(\frac{E_o}{E_i} \right)^{-0.32} \left(\frac{E_o}{E_e} \right)^{0.06} \left(\frac{h_o}{h_i} \right)^{0.13} \times \left(\frac{h_o}{h_e} \right)^{0.04} \left(\frac{kh_o}{E_o} \right)^{0.48} \left[2.8756 \left(\frac{h_o}{L} \right)^2 - 0.1911 \left(\frac{h_o}{L} \right) + 0.0050 \right] \quad (8b)$$

For $h_o = 15.24$ cm:

$$\frac{P_{ult}}{bh_o f_{io}} = 10^4 \left(\frac{h_o}{l_{cho}} \right)^{-0.60} \left(\frac{h_i}{l_{chi}} \right)^{0.51} \left(\frac{E_o}{E_i} \right)^{-0.33} \left(\frac{E_o}{E_e} \right)^{0.07} \left(\frac{h_o}{h_i} \right)^{0.12} \times \left(\frac{h_o}{h_e} \right)^{0.05} \left(\frac{kh_o}{E_o} \right)^{0.41} \left[1.0627 \left(\frac{h_o}{L} \right)^2 - 0.0785 \left(\frac{h_o}{L} \right) + 0.0025 \right] \quad (8c)$$

For $h_o = 17.78$ cm:

$$\frac{P_{ult}}{bh_o f_{io}} = 10^3 \left(\frac{h_o}{l_{cho}} \right)^{-0.59} \left(\frac{h_i}{l_{chi}} \right)^{0.48} \left(\frac{E_o}{E_i} \right)^{-0.33} \left(\frac{E_o}{E_e} \right)^{0.07} \left(\frac{h_o}{h_i} \right)^{0.11} \\ \times \left(\frac{h_o}{h_e} \right)^{0.07} \left(\frac{kh_o}{E_o} \right)^{0.34} \left[3.8264 \left(\frac{h_o}{L} \right)^2 - 0.3043 \left(\frac{h_o}{L} \right) + 0.0118 \right] \quad (8d)$$

For $h_o = 20.32$ cm:

$$\frac{P_{ult}}{bh_o f_{io}} = 10^3 \left(\frac{h_o}{l_{cho}} \right)^{-0.53} \left(\frac{h_i}{l_{chi}} \right)^{0.51} \left(\frac{E_o}{E_i} \right)^{-0.32} \left(\frac{E_o}{E_e} \right)^{0.07} \left(\frac{h_o}{h_i} \right)^{0.11} \\ \times \left(\frac{h_o}{h_e} \right)^{0.07} \left(\frac{kh_o}{E_o} \right)^{0.30} \left[2.1634 \left(\frac{h_o}{L} \right)^2 - 0.1798 \left(\frac{h_o}{L} \right) + 0.0082 \right] \quad (8e)$$

These equations are plotted in Fig. 8 together with the results of the simulations and with the results of simulations performed for random choices of the parameters within the stated ranges. The agreement between the regressions and the simulations is deemed acceptable for all intents and purposes. It is noted the exponent of each dimensionless variable is not a strong function of the overlay thickness. However, the polynomial functions of the pavement aspect ratio differ significantly from thickness to thickness.

The ultimate capacity equations can be further simplified for the practical range considered in this paper by noting that the exponents associated with E_o/E_e and h_o/h_e are nearly zero. The weak dependence of the ultimate load capacity on the stiffness and thickness of the existing pavement is in contrast with the currently available design formulas, which state that thicker existing pavements require thinner UBCOs. It is noted that fracture mechanics-based design equations that may eventually be developed should be conservative. Therefore, equations similar to those listed previously will be used that bound all of the simulations listed subsequently.

Eq. (8) also sheds insights on how to improve the ultimate capacity of UBCOs that fail as a result of reflection cracking. It suggests that the load capacity is most sensitive to h_o/l_{cho} and h_i/l_{chi} . Therefore, the most effective ways of increasing capacity are to increase the toughness (actually the tensile strength because the critical crack opening displacement is assumed to be a constant value) of the overlay and/or the interlayer. Increasing the foundation stiffness k , and/or increasing the thickness of the interlayer h_i , and/or decreasing the stiffness of the interlayer E_i also result in increased ultimate capacity.

The influence of the overlay length L is not monotonic because the separation between the UBCO pavement and the foundation is not considered. When h_o/L is relatively large, there is no separation and the foundation is in full compression. The load capacity decreases as L increases. However, when L increases beyond a certain length, the foundation at the ends of the pavement is required to carry relatively small tension forces to maintain contact, and these result in an increase in the ultimate capacity. If there is sufficient adhesion between the pavement and the foundation, then this increase can be achieved. If not, then a more complex moving boundary problem simulation is required to determine the effects of the layer aspect ratio.

Structural Equivalency Design of UBCOs

The following procedure is proposed as an illustration of how fracture mechanics can be used as the basis of UBCO design procedures.

1. For a chosen set of material and foundation properties, determine the thickness of a new single-layer pavement that is required to meet the service requirements. The requirements may include various thermomechanical loadings and cracking scenarios.
2. Using Eq. (7), determine the load capacity of the single-layer pavement.
3. Using Eq. (8), select a combination of material properties and geometric configurations, then determine the load capacities of the UBCO systems for 10.16- to 20.32-cm-thick overlays.
4. Select the required UBCO thickness to render the UBCO structurally equivalent to the single-layer pavement.

This procedure is illustrated for $L = 6.10$ m, $k = 27.14$ MPa/m, $h_i = 2.54$ cm, $h_e = 20.32$ cm, $E_o = 27.58$ GPa, $E_e = 34.47$ GPa, $f_{io} = 2.76$ MPa, and $G_{Fo} = 105.08$ N/m. Assuming the required thickness of a new single-layer pavement is 20.32 cm and its material properties are the same as those of the overlay, Eq. (7) predicts its capacity as 2.10 kN (the *ABAQUS* simulation of this case predicts a capacity equal to 2.09 kN). Assuming AC interlayer properties $E_i = 3.45$ GPa and $f_{ii} = 4.14$ MPa, Eq. (8) predicts the load capacities for 10.16-, 12.70-, 15.24-, 17.78-, and 20.32-cm-thick overlays are 1.71, 1.85, 2.04, 2.24, and 2.53 kN, respectively. Therefore, the 20.32-cm-thick single-layer pavement is equivalent to an UBCO with an overlay thickness approximately equal to 16.51 cm (by interpolation). If the properties are changed to $E_i = 3.45$ GPa and $f_{ii} = 3.45$ MPa, then the required overlay thickness becomes 18.29 cm; thus, illustrating that the interaction between the overlay and the interlayer is significant and cannot be neglected as is done by the currently used MnDOT (1993) procedures. The two currently available procedures described in the appendix require, respectively, a constant 16.51- or 17.27-cm-thick overlay for poor existing pavement conditions regardless of the properties of the interlayer.

The previous examples drive home the point that the usefulness of the fracture mechanics modeling lies in its ability to enable the designer to explore the effects of all of the material and geometric parameters on the required thickness of the overlay. If the values of the material and geometric parameters fall outside the ranges investigated in this paper, the same process carried out here can be repeated to develop similar design equations. Eventually, fracture mechanics-based design guidelines could be developed that account for all possible loadings, temperature conditions, etc. With proper choices of material properties and geometric parameters, thinner overlay thicknesses may be achieved.

Comparison with Field Study

In July 2010, the writers observed the condition of the four UBCO test sections built in 2008 at the MnROAD test facility located parallel to westbound Interstate Highway I-94 near Albertville, Minnesota. The dimensions of the cells, numbered 105, 205, 305, and 405, are shown in the schematic in Fig. 9; the thickness of the AC interlayer of all sections was 2.54 cm. Also shown in Fig. 9 is an image representative of the cracking that was observed in all sections 25–50 cm from the cell-separating joints. These cracks were not reflective. Instead they were attributed to temperature effects such as curling or warping.

Most importantly, no other cracks were observed within the overlays. This suggests that the thicknesses of the overlays were

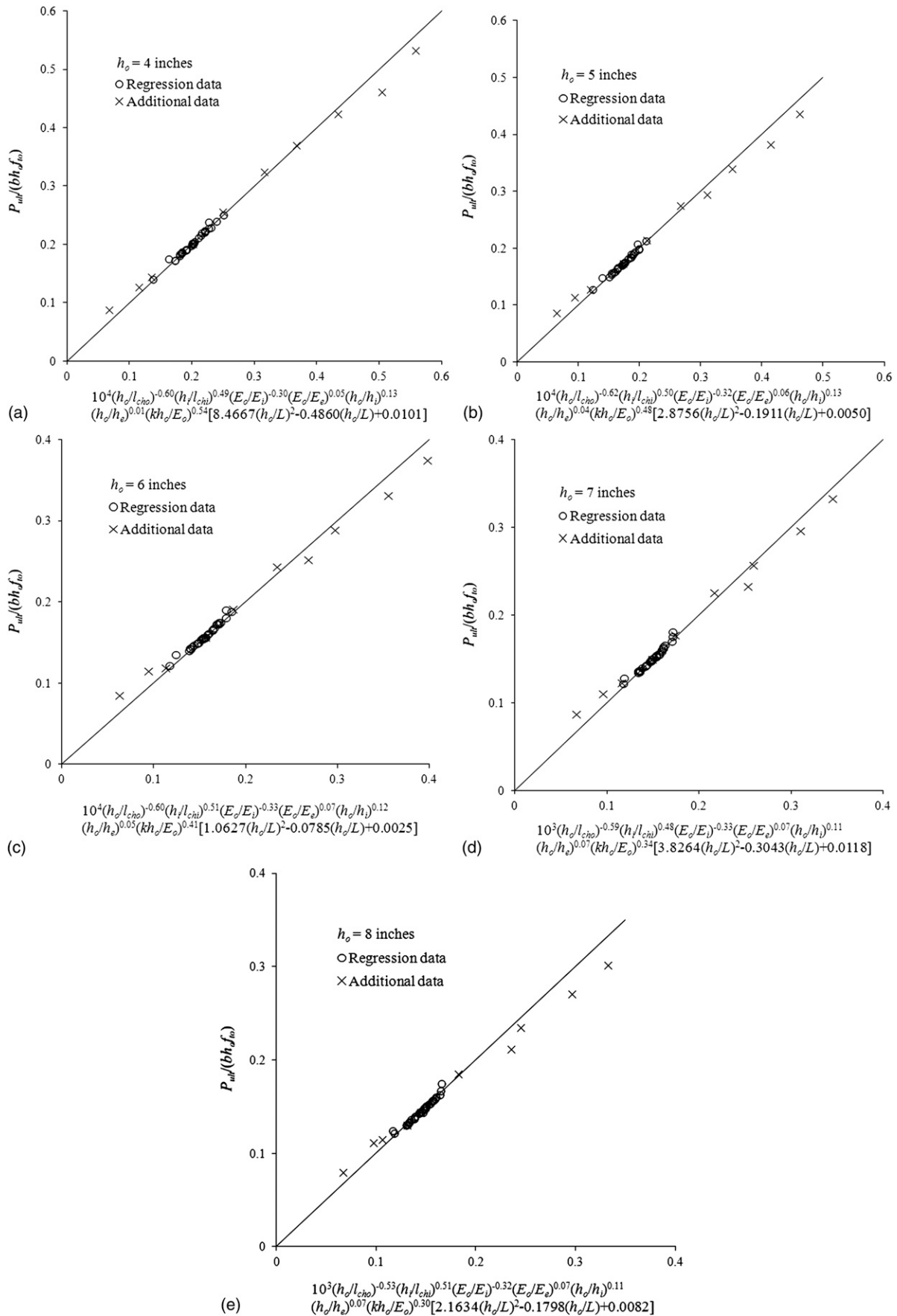


Fig. 8. Derived relationship between the capacity and the variables: (a) $h_o = 10.16$ cm; (b) $h_o = 12.70$ cm; (c) $h_o = 15.24$ cm; (d) $h_o = 17.78$ cm; (e) $h_o = 20.32$ cm

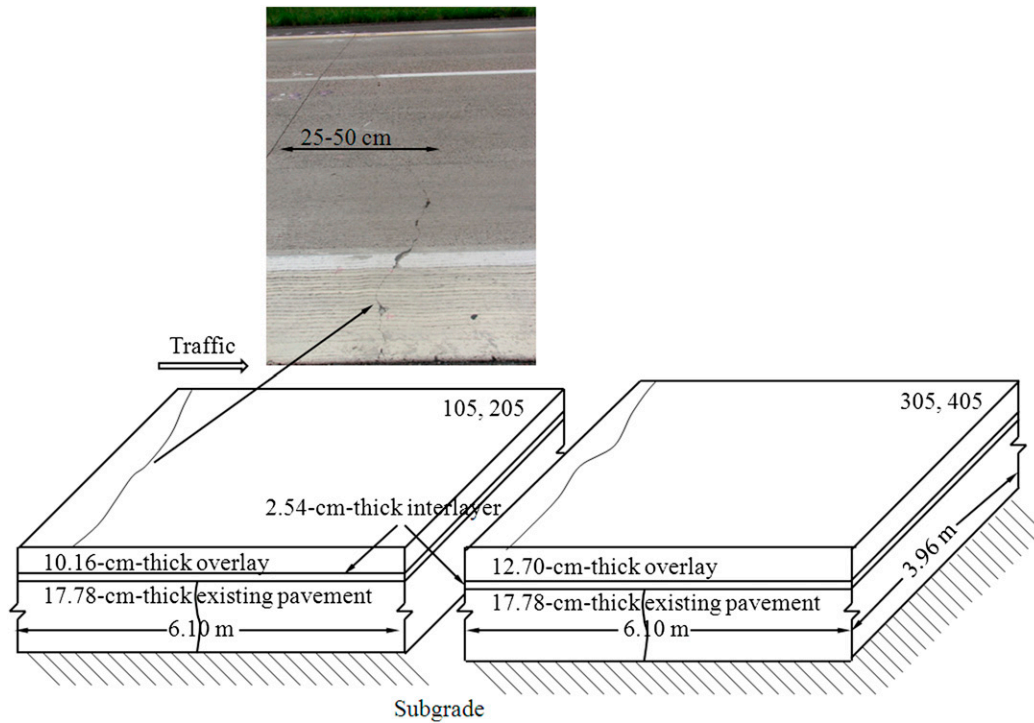


Fig. 9. MnROAD test sections of UBCOs

sufficient to resist the potential reflection cracking considered in this paper. The developed models cannot be directly applied to interpret the MnROAD section because the material parameters of the section were not known to the writers. Furthermore, the temperature, moisture, and traffic effects were not considered in the model. Further research is suggested to consider these effects in the future. Nevertheless, assuming the practical values of the parameters— $E_o = 27.58$ GPa, $E_i = 3.45$ – 10.34 GPa, $E_e = 34.47$ – 62.05 GPa, $f_{io} = 2.76$ – 4.14 MPa, $f_{ii} = 2.76$ – 4.14 MPa, $G_{Fo} = 105.08$ – 157.61 N/m, $G_{Fi} = 262.69$ – 394.04 N/m, and $k = 27.14$ MPa/m—Eqs. (7) and (8) state that the originally designed 17.78-cm-thick single-layer pavement is structurally equivalent to a minimum overlay thickness of 12.19 cm. Therefore, Overlays 105 and 205 tested at MnROAD (even though they were 2 cm thinner than the lower bound suggested by the fracture mechanics–based design approach) appear to be of sufficient thickness to mitigate reflection cracking. These observations reinforce the notion that the simplified assumptions, such as plane strain deformation and zero joint load transfer efficiency, may lead to conservative values of required overlay thickness. Moreover, these observations suggest that experiments be performed to determine whether currently used design formulas are conservative [a minimum overlay thickness of 15.24 cm is required by MnDOT (1993)], and whether thinner overlays may prove to be sufficiently robust. Additional fracture mechanics modeling (including three-dimensional simulations that represent more realistically the geometry and loading conditions associated with UBCOs), together with carefully chosen experimental configurations, should provide additional insights as to whether UBCOs can be “thinned-up.”

Conclusions

Nonlinear fracture mechanics has been applied for the first time to the analysis of UBCOs. The developed fracture mechanics–based

design paradigm offers promise for improved design of UBCOs. The CZM approach allows, for a given value of overlay thickness, the ultimate load-carrying capacity to be expressed as a combination of a power law and polynomial function of all the fundamental material and geometric parameters that describe the composite pavement system. The resulting formulas can enable the pavement designer to optimize the combination of material properties and geometric dimensions to achieve a desired equivalency between the UBCO and a reference single-layer PCC pavement. Increasing the toughness (actually, the strength, because the critical crack opening displacement in the illustrative examples is maintained constant) of the interlayer and/or the overlay and decreasing the stiffness of the interlayer are some of the most effective ways of improving the load-carrying capacity of the UBCO pavement. This result is consistent with the pavement community’s recent focus on the development of various types of interlayer systems to improve performance of UBCO pavements.

Appendix. Summary of the Two Design Procedures Currently Used by MnDOT for UBCOs

Departments of the Army and the Air Force (DA/DAF 1970) Design Procedure

This procedure is based on an empirical equation that requires the PCC overlay to satisfy a structural deficiency between the required thickness for a new single-layer PCC pavement resting on the same subgrade and the thickness of the existing PCC pavement. The design equation is

$$h_o = \sqrt{h_n^2 - Ch_e^2} \quad (9)$$

where h_n = thickness that would be required for a new single-layer PCC pavement resting on the same subgrade, and C = constant that

depends on the condition of the existing PCC pavement. The recommended values for C are 1.00 when the existing pavement is in good condition with little or no structural cracking; 0.75 when the existing pavement has a few initial structural crackings but no progressive cracking; and 0.35 when the existing pavement is badly cracked.

Tayabji and Okamoto (1985) Design Procedure

This procedure is based on finite-element-method-based mechanistic models. The existing PCC pavement and the PCC overlay are treated as distinct slabs resting on the subgrade. The analysis is conducted for the following conditions: 6.10-m-long joint spacing of overlays, 80 kN single axle load, 34.47 GPa of the overlay's Young's modulus, 20.68–27.58 GPa of the existing pavement's Young's modulus, and 27.14–81.43 MPa/m of the foundation stiffness. The procedure is based on a stress equivalency concept as illustrated in Fig. 1. The design demands that the critical stress that develops in the PCC overlay is no larger than the stress that would be acceptable in a new single-layer PCC pavement resting on the same subgrade. Finally, the procedure presents three design charts that determine the PCC overlay thickness for the following three cases: (1) the existing pavement exhibits a large amount of midslab and corner cracking with poor load transfer at the joints and cracks; (2) the existing pavement exhibits a small amount of midslab and corner cracking with reasonably good load transfer at the joints and cracks; and (3) the existing pavement exhibits a small amount of midslab cracking with good load transfer at the joints and cracks.

Acknowledgments

The writers acknowledge support from the Minnesota Department of Transportation, the James L. Record Chair, the Minnesota Supercomputing Institute, and discussions with Dr. Lev Khazanovich.

References

Bazant, Z. P. (2002). "Concrete fracture models: Testing and practice." *Eng. Fract. Mech.*, 69(2), 165–205.

- Bazant, Z. P., and Novak, D. (2001). "Proposal for standard test of modulus of rupture of concrete with its size dependence." *ACI Mater. J.*, 98(1), 79–87.
- Bazant, Z. P., and Planas, J. (1998). *Fracture and size effect in concrete and other quasibrittle materials*, Section 9.3, CRC, Boca Raton, FL.
- Boresi, A. P., and Schmidt, R. J. (2003). "Beams on elastic foundations." *Advanced mechanics of materials*, 6th Ed., Wiley, Hoboken, NJ, 357–378.
- Buckingham, E. (1914). "On physically similar systems: Illustrations of the use of dimensional equations." *Phys. Rev.*, 4(4), 345–376.
- Dassault Systèmes Simulia Corporation (SIMULIA). (2010). *ABAQUS 6.10 documentation*. Dassault Systèmes Simulia Corporation, Providence, RI.
- Departments of the Army and the Air Force (DA/DAF). (1970). "Rigid pavements for airfields other than army." *Technical manual 5-824-3/Air Force manual 88-6*, Chapter 3, DA/DAF, Washington, DC.
- Engstrom, G. M. (1993). "Unbonded concrete overlays: Minnesota experience." *Interim Rep.*, Engineering Services Division, Office of Materials and Research, Physical Research Section, Minnesota Department of Transportation, Saint Paul, MN.
- Hilsdorf, H. K., and Brameshuber, W. (1991). "Code-type formulation of fracture mechanics concepts for concrete." *Int. J. Fract.*, 51(1), 61–72.
- Ioannides, A. M., and Sengupta, S. (2003). "Crack propagation in portland cement concrete beams: Implications for pavement design." *Transportation Research Record 1853*, Transportation Research Board, Washington, DC, 110–117.
- Liao, M. (2011). "Towards fracture mechanics-based design of unbonded concrete overlay pavements." Ph.D. dissertation, Univ. of Minnesota, Minneapolis.
- Minnesota Department of Transportation (MnDOT). (1993). "Unbonded concrete overlay design procedure." Office of Materials Research and Engineering, Pavement Engineering Section, MnDOT, Saint Paul, MN.
- Petersson, P.-E. (1981). "Crack growth and development of fracture zones in plain concrete and similar materials." *Rep. TVBM-1006*, Division of Building Materials, Lund Institute of Technology, Lund, Sweden.
- Roesler, J., Paulino, G. H., Park, K., and Gaedicke, C. (2007). "Concrete fracture prediction using bilinear softening." *Cem. Concr. Compos.*, 29(4), 300–312.
- Tayabji, S. D., and Okamoto, P. A. (1985). "Thickness design of concrete resurfacing." *Proc., 3rd Int. Conf. on Concrete Pavement Design and Rehabilitation*, Purdue Univ., West Lafayette, IN, 367–379.
- Westergaard, H. M. (1947). "New formulas for stresses in concrete pavements of airfields." *Trans. Am. Soc. Civ. Eng.*, 73(5), 687–701.
- Wittmann, F. H., Rokugo, K., Brühwiler, E., Mihashi, H., and Simonin, P. (1988). "Fracture energy and strain softening of concrete as determined by means of compact tension specimens." *Mater. Struct.*, 21(1), 21–32.

Copyright of Journal of Engineering Mechanics is the property of American Society of Civil Engineers and its content may not be copied or emailed to multiple sites or posted to a listserv without the copyright holder's express written permission. However, users may print, download, or email articles for individual use.